Functionalized Carbon Black Supported Silver (Ag/C) Catalysts in Cathode Electrode for Alkaline Anion Exchange Membrane Fuel Cells

Van Men Truong, Ming-Kun Yang & Hsiharng Yang

International Journal of Precision Engineering and Manufacturing-Green Technology

ISSN 2288-6206
Volume 6
Number 4

Int. J. of Precis. Eng. and Manuf.-Green Tech. (2019) 6:711-721
DOI 10.1007/s40684-019-00123-3

Springer

International Journal of Precision Engineering and Manufacturing-Green Technology (2019) 6:711–721
https://doi.org/10.1007/s40684-019-00123-3

Online ISSN 2198-0810
Print ISSN 2288-6206

REGULAR PAPER

Functionalized Carbon Black Supported Silver (Ag/C) Catalysts in Cathode Electrode for Alkaline Anion Exchange Membrane Fuel Cells

Van Men Truong[1] · Ming-Kun Yang[1] · Hsiharng Yang[1,2]

Received: 11 December 2018 / Revised: 2 June 2019 / Accepted: 3 June 2019 / Published online: 12 June 2019

Abstract
Two kinds of non-platinum metal catalysts, 40 wt% Ag/C (Ag/C) prepared using the impregnation method and commercial nano-silver powder (commercial Ag) were used as the cathode catalysts in alkaline anion exchange membrane fuel cells (AEMFC). In the surface measurement and elemental composition analysis of the prepared Ag/C catalyst, XRD revealed that the silver nanoparticles were successfully produced and attached onto the carbon black supporter. In addition, SEM and TEM analyses showed the silver nanoparticle size catalyst was less than 20 nm in the synthesized Ag/C. EDX and TGA analyses confirmed that the actual Ag loading in the Ag/C catalyst was near the calculated value in the synthesis procedure. For AEMFC performance tests, the results showed that the maximum power densities using Ag/C, commercial Ag, and Pt/C as the cathode catalysts were 200 mW cm^{-2} at 0.4 V, 105 mW cm^{-2} at 0.3 V, and 207 mW cm^{-2} at 0.5 V which were consistent with the CVs and LSV characterizations. These results indicated that the performance of tested AEMFC with Ag/C and commercial Ag catalysts was 3.5% and 49.3% less than that of AEMFC with Pt/C, respectively. This study successfully implemented non-Pt catalyst for the cathode electrode in AEMFC applications.

Keywords Alkaline anion exchange membrane fuel cell · Carbon black · Nano-silver · Non-platinum catalysts · Oxygen surface groups

1 Introduction

Fuel cells have been widely considered efficient with very low pollutant emission power due to their high energy conversion efficiency and high power density compared with the conventional internal combustion system [1–3] Several types of fuel cells generally characterized by employed electrolyte material such as polymer exchange membrane fuel cells including proton exchange membrane fuel cells and anion exchange membrane fuel cells [4–6], molten carbonate fuel cells [7, 8], solid oxide fuel cells [9–11], phosphoric acid fuel cells [12] and alkaline fuel cells [13] have been recently developed and used in many applications depending on their advantages and limitations. Among low-temperature fuel-cell types, anion exchange membrane fuel cells (AEMFCs) have received extensive attention owing to their advantages compared to the proton exchange membrane fuel cells (PEMFCs). The key advantage is the possibility of using non-noble metals as electrode catalysts due to faster oxygen reduction reaction (ORR) kinetics in alkaline media than in acidic media [14, 15] and a less corrosive environment for electrodes, which are the main hindrance of PEMFCs. Additionally, the power generated by a fuel cell depends mainly on the catalytic electrodes and materials used [16, 17].

The AEMFC operating principle is similar but not identical to that of PEMFCs. In AEMFCs, water is generated at the anode from the HOR while this happens at the cathode from the ORR in PEMFCs. Water also takes part in an electrochemical reaction consumed at the cathode by the ORR. Figure 1 shows the typical AEMFC schematic diagram based on a similar sandwich structure composed of an anode electrode, membrane, and cathode electrode. The

✉ Hsiharng Yang
hsiharng@nchu.edu.tw

[1] Graduate Institute of Precision Engineering, National Chung Hsing University, 145 Xingda Road, South District, Taichung City 402, Taiwan

[2] Innovation and Development Center of Sustainable Agriculture (IDCSA), National Chung Hsing University, 145 Xingda Road, South District, Taichung City 402, Taiwan

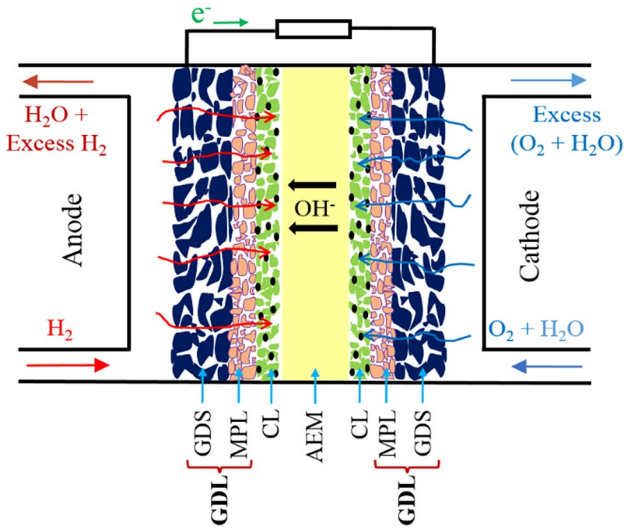

Fig. 1 Schematic diagram of anion exchange membrane fuel cell

electrochemical reactions occur across the entire catalyst layers in an AEMFC as described below:

$$\text{At anode}: 2H_2 + 4OH^- \; 4H_2O + 4e^-; E^0 = -0.828\ V. \tag{1}$$

At cathode, the reduction of O_2 can proceed by two pathways, the so-called direct four-electron pathway and two-electron pathway (or indirect four-electron pathway) in alkaline media [18]:

Direct four-electron pathway

$$O_2 + 2H_2O + 4e^- 4OH^-; E^0 = 0.401\ V. \tag{2}$$

Two-electron pathway

$$O_2 + 2H_2O + 2e^- HO_2^- + OH^-; E^0 = -0.065\ V. \tag{3}$$

Thereafter, the unstable peroxides radical HO_2^- can either be further reduced

$$HO_2^- + 2H_2O + 2e^- 3OH^-; E^0 = 0.867\ V, \tag{4}$$

or decomposed by a chemical disproportionation reaction

$$2HO_2^- 2OH^- + O_2, \tag{5}$$

and the O_2 molecule can be recycled through the first ORR step. One of the strategy in developing effective catalysts toward ORR is to promote a direct four-electron pathway, to yield an efficient reduction of O_2, and lower overpotential compared to an undesired two-electron pathway [19, 20].

In alkaline media, the electrocatalyst activity is higher than that in acid media due to enhanced ion transport and facile charge transfer. In addition, the poisoning effects on catalysts are also weak, and a wider range of metals are stable in an alkaline environment. Thus, non-Platinum group metals can be used as electrocatalysts [21, 22].

Silver (Ag) has been recognized as a promising cathode catalyst for a long time due to its high oxygen reduction reaction (ORR) activity at high pH and relatively high stability in a wide range of temperatures [23, 24]. For instance, Chatenet et al. [25] found that the ORR activity on Ag is close to that on Pt in high concentration alkaline media. Wang et al. [26] reported that the silver-molybdate electrocatalyst was successfully prepared using the hydrothermal method. The synthesized silver-molybdate electrocatalyst exhibited higher catalytic activity for ORR and better durability than Pt/C catalyst in alkaline solution. Meng et al. [27] reported on a 4-electron pathway with regard to carbon supported large particles (i.e. > 20 nm). In addition, the price of Ag is much lower (about 75 times) than that of precious metal Pt. These merits make Ag a potential candidate for applications in alkaline fuel cells and metal–air batteries. Blizanac et al. [28] investigated the ORR on Ag single-crystal surfaces using rotating ring-disk technique in alkaline solution over the temperature range 293–333 K. Their result showed that the ORR proceeds through the $4e^-$ reaction pathway with a very small (≈0.5 to 2%) peroxide formation at all tested temperature. Han et al. [29] also found that the ORR proceeded along two parallel reaction pathways on the Ag/C catalyst. The four-electron reduction of O_2 occurs on larger Ag particles (174 nm) while the finer Ag particles (4.1 nm) are favorable to the two-electron reduction of O_2. Xin et al. [30] reported that the 4-electron pathway of ORR proceeds on small Ag nanoparticles (2–9 nm) via a four-electron transfer process and suggested ORR activities of the prepared Ag/C and a commercial Pt/C were comparable. Amanda et al. [31]. presented that the number of electrons exchanged by O_2 molecules on carbon-supported Ag nanoparticles (around 20 nm) estimated using Levich plot was 2.7 per O_2. They concluded that the ORR may simultaneously occur at the Ag sites by a four-electron pathway and at the carbon sites by a two-electron mechanism. Moreover, some researchers have studied the Ag-based catalyst synthesis to replace Pt/C for ORR in AEMFCs. For example, Vinodh et al. [32] synthesized carbon supported silver catalyst (Ag/C) with Ag loading from 2 to 10 wt% using the wet impregnation method. Their results showed that the prepared Ag particles were in the nanometer range and stable even at 800 °C. Similar work was performed by Maheswari et al. [33]. Ag/C in varying percentages, namely, 40, 60, and 80% were prepared using the sodium citrate protection method and 60% Ag/C showed better AEMFC performance than two other loads consistent with the kinetic data in half-cell studies. Wang et al. [34] investigated the effect of Ag particle size on ORR in anion exchange membrane direct glycerol fuel cell. Smaller Ag particle size had higher ORR activity and then, exhibited better cell performance.

There have been numerous strategies proposed to improve the electrocatalyst performance for fuel cell devices. Among them, modification of support materials via physical/chemical treatment or addition of suitable materials to have better interaction between metal catalysts and supports such as more uniform distribution of metal catalysts with smaller nanoparticle sizes, increase in electrochemical active area, higher stability and durability has been preferred. For example, Arukula et al. [35] successfully synthesized rGO/PANI/Pt–Pd composite using a wet reflux strategy for methanol oxidation. They reported that the presence of PANI are beneficial for tuning the surface of rGO to allow a uniform dispersion of Pt–Pd nanoparticles and generating strong interaction with Pt–Pd through nitride bond and thereby, significant enhance catalytic activity and durability for methanol oxidation in alkaline media compared to Pt/C. The direct methanol fuel cell testing showed that the peak power density of using the rGO/PANI/Pt–Pd catalyst was approximately two times higher than that of using Pt/C. Ramakrishman et al. [36] demonstrated that the flower structure of MoS_2/N-doped reduced graphene oxide (MoS_2/NrGO) obtained by hydrothermal method can help strengthen the anchoring of ultrafine Pt nanoparticles because of the electrostatic interaction between MoS_2/NrGO and Pt.In comparison to Pt@/NrGO and Pt/C, their cyclic voltammetry results showed that the Pt@MoS_2/NrGO catalyst exhibited an excellent catalytic activity and stability towards alcohol oxidation reaction and ORR suitable for direct alcohol fuel cells. For a long time, it is well known that the interaction between the metal ion and carboxylic acid group (–COOH) plays an important role for several applications, especially, in the field of environmental science and catalysis [37]. For example, the selective removal of toxic metal ions in wastewater treatment has been effectively obtained from the interaction of polycarboxylates with metal ions [38]. Furthermore, introducing surface functional groups is favorable for the metal dispersion of many carbon-supported metal catalysts [39]. Increasing oxygen functional groups on activated carbon could increase the adsorption of metal ions [40, 41]. These characteristics were utilized to increase the metal catalyst loads on an activated carbon support. Introducing oxygen-containing functional groups onto the carbon surface could be implemented by mechanical [42], chemical [43], and electrochemical routes [44]. Carbon support treated with HNO_3 to create surface functional groups (e.g. –COOH, –OH) [45–47], was investigated by some research groups. For example, Erhan Aksoylu et al. [48] reported that the pretreatment of activated carbon supports with 5 N HNO3 was able to improve the Pt dispersion from 13% up to 92% compared to the fresh Pt/C catalyst. Xiong et al. [49] reported that the Niobia catalyst load increased on activated carbon support pretreated with 50% HNO_3 solution to generate functional groups on its surfaces. In addition, the Niobia/carbon catalyst was much more hydrothermally stable which can be attributed to the formation of nano-sized niobia particles and a strong interaction between niobia and carbon. Similar results were also obtained for different metal catalysts on activated carbon support [50, 51]. Moreover, it is also known that the surface modification of activated carbon increases its hydrophilicity which is also useful for electrocatalysts.

Owing to the benefits of functional groups on carbon support surfaces and the low cost and availability of carbon black (Vulcan XC-72R), this work aims at using a commercial Vulcan XC-72R carbon black which undergoes a surface modification with nitric acid (HNO_3) to enhance the metal absorption as catalyst supporter. In addition, silver is also chosen as a metal reduction catalyst due to its potential in alkaline media as mentioned above to synthesize carbon black supported silver (Ag/C) for use as ORR in AEMFCs. The functional groups were formed after the chemical modification is confirmed using FTIR spectrophotometer. The Ag/C is then simply synthesized using the wet impregnation method and physically and chemically characterized. The prepared Ag/C catalyst activities toward AEMFC performance will be evaluated in comparison with commercial Pt/C.

2 Experimental

2.1 Ag/C Catalyst Synthesis

A commercial carbon black (CB) Vulcan XC-72R (Cabot) was used as a support. This carbon was functionalized with 20% HNO_3 at 120 °C, refluxed for 2 h. After that, the functionalized carbon was filtered and washed with DI water until filtrate neutralization was reached, followed by drying at 110 °C overnight.

Silver supported on carbon black was prepared using the wetness impregnation method as follows. First, 123.3 mL of 50 mM $Na_3C_6H_5O_7$ was prepared and 123.3 mL of 10 mM$AgNO_3$ was added. Sodium citrate, inhere, was used to prevent the silver particle agglomeration during the reduction step. Next, 167 mL of 7.4 mM $NaBH_4$ was added dropwise under a vigorously stirring condition. After that, 200 mg of modified Vulcan XC-72 carbon black were dispersed into the Ag colloid. Next, the suspension was stirred for 12 h before filtering and washing with DI water several times to reach a neutral pH. The catalyst was then dried in an oven at 80 °C for 12 h. The collected catalyst power was named as 40 wt% Ag/C.

2.2 Synthesized Catalyst Characterization

The presence of oxygen-containing functional groups (O=C–OH and C–OH) on the CB surfaces treated with nitric acid was identified using Fourier Transform Infrared Spectroscopy (FTIR, Agilent Cary 630 FTIR Spectrometer G8043-64001). The chemical composition and crystallographic structure of the as-synthesized catalyst materials were characterized using scanning electron microscopy (SEM, JSM-6700F), high-resolution X-ray diffractometer (HRXRD, BRUKER D8 SSS), high resolution transmission electron microscopy (HRTEM, JEOL JEM-2010), and Energy Dispersive X-Ray (EDX). Thermogravimetric analysis (TGA) was also carried out using the PerkinElmer STA 6000 model at a heating rate of 10 °C/min from room temperature to 930 °C under nitrogen (N_2) and O_2 environments.

In addition, for electrochemical characterization, cyclic voltammetry (CV) measurements were conducted in 1 M KOH solution using Zahner Zennium E workstation in a three-electrode configuration. A glassy carbon electrode (GCE) with a geometric area of 0.071 cm [2], an Ag/AgCl (0.196 V vs. SHE), and a Pt wire were used as the working electrode, reference electrode, and counter electrode, respectively. Before each test, the GCE working surface was polished with a 0.05 µm alumina slurry on a polishing pad for 5 min, followed by rinsing with deionized (DI) water in an ultrasonic bath for 20 min. The catalyst ink was prepared by mixing the catalyst with DI water, isopropyl alcohol (IPA) and aQAPS-S_{14} ionomer (supplied by Hephas Energy Co., Ltd). For instance, to prepare the Ag/C catalyst ink, 6.21 mg of Ag/C catalyst powder were dispersed into 9.5 mL DI water, followed by adding 9.5 mL of IPA and 100 µL of the ionomer. The mixture was sonicated for 1 h. The catalyst ink was drop-casted on the GCE surface with the loading of 35.0 μg_{Ag} cm^{-} [2] and dried at room temperature (~ 27 °C). Linear sweep voltammetry (LSV) experiments were conducted in O_2-saturated 1 M KOH using rotating disk electrode (RDE, geometric area of 0.196 cm [2]) which was prepared in the same procedure as the GCE. All CV and LSV experiments were performed at room temperature (~ 27 °C).

2.3 Fuel Cell Test

The anion exchange membrane (AEM) and ionomer used in this work were aQAPS-S_8 and aQAPS-S_{14} (supplied by Hephas Energy Co., Ltd), respectively. The aQAPS-S_8 membrane with a thickness of 30–40 µm in the dry form has an ion exchange capacity (IEC) of ca. 1.0 meq g^{-1} and specific ion conductivity of ca. 0.1 S cm^{-1} at 60 °C. The main aQAPS-S_8 membrane structure is composed of quaternary ammonium groups with the hydrophobic side chains attached to the polysulfone backbone to obtain the ion-aggregating structure that is beneficial for ion conductivity. As the membrane was available in chloride form (Cl^{-}), pre-treatment was performed to convert it into the hydroxide form (OH^{-}) by soaking for 24 h in 1 M KOH. The prepared electrodes were also dipped in 1 M KOH solution to transform the binder from Cl^{-} into OH^{-} form. The GDL-280 carbon paper with a thickness of 280 µm (supplied by CeTech Co., Ltd., Taiwan) was selected as the gas diffusion layer in both the anode and cathode sides.

The catalyst ink was prepared by blending Pt/C (40 wt% Pt, Tanaka) or preparing 40 wt% Ag/C powder with 25 wt%. aQAPS-S_{14} ionomer (2 wt% DMF, Alfa Aesar) and the DI water and IPA (Isopropyl alcohol) mixture with a volumetric ratio of 1:1 DI water/IPA as the dispersant/solvent. The catalyst ink was sonicated for 60 min to promote homogenization and then coated onto the MPL GDL surface by hand-brushing on a hot plate at 80 °C. The catalyst loads of 40 wt% Pt/C, 40 wt% Ag/C and commercial Ag nanoparticles were 0.8 mg cm^{-2}, 1.0 mg cm^{-2}, and 3.0 mg cm^{-2}, respectively.

Finally, the aQAPS-S_8 membrane was sandwiched between the two electrodes without hot pressing. The active electrode area was 25 cm [2]. The MEA was secured between two graphite plates with machined triple serpentine flow channels (1 mm channel width, 1 mm channel height, and 1.5 mm rib width) and gold coated copper current collector plates with gaskets. Teflon gaskets with a thickness of 220 µm were used to give 20–30% GDL compression. The fixture was then sealed using 8 bolts with a constant torque of 1.47 Nm. A fuel cell testing system (FCED-PD50 test station, Asia Pacific Fuel Cell Technologies, Ltd.) was operated at a cell temperature of 50 °C with humidified H_2 and O_2 fed at flow rates of 1.0 and 0.5 slpm and dew points of 50 °C and 55 °C, respectively.

3 Results and Discussion

3.1 Synthesized Catalyst Characteristics

FT-IR spectra conducted on pristine and functionalized CB with nitric acid treatment in the range 1000–4000 cm^{-1} are shown in Fig. 2. The observed band around 3430 cm^{-1} corresponds to O–H stretching vibration from moisture absorption, hydroxyl groupsor carboxyl grouposcillation present in the samples [52, 53]. Note that hydroxyl groups or carboxyl groups on the surfaces of untreated CB could be attributable to the partial oxidation of CB surfaces during purification by the manufacturer. The peak observed at ~ 1600 cm^{-1} arises from the C=C stretching vibrations of graphite band (G-band) [54]. In addition, after treatment, the peak observed at 2925 cm^{-1} corresponds to the H–C stretch modes of H–C=O in the carboxyl group. Furthermore, a new peak also appears from the CB–COOH at 1256 cm^{-1} [55].

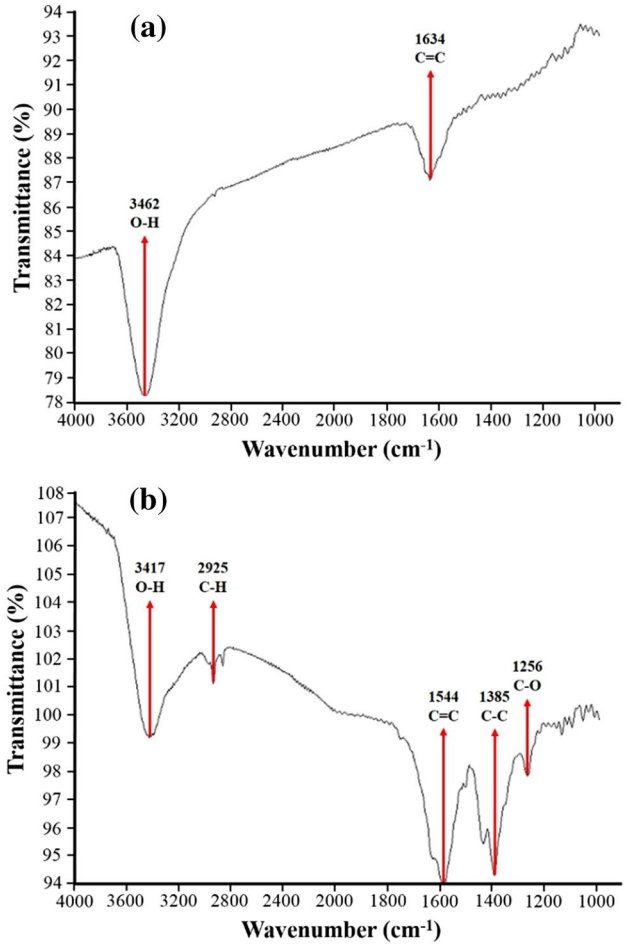

Fig. 2 FT-IR spectra of carbon black: **a** Before surface modification; **b** After surface modification

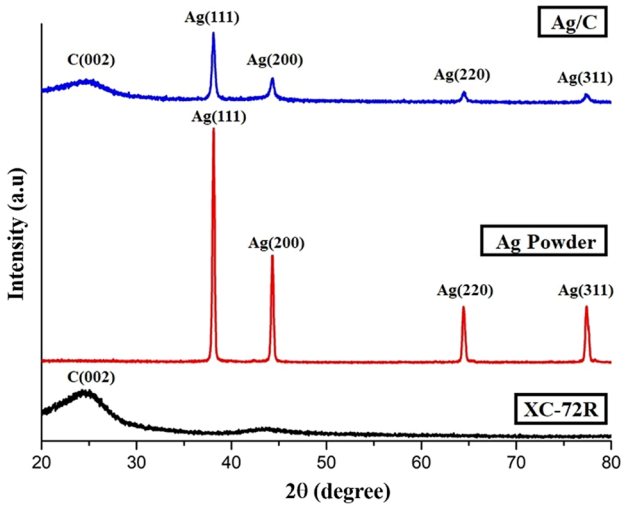

Fig. 3 XRD spectrum patterns

This peak is assigned to C–O bonding. The peak observed at 1385 cm^{-1} can be ascribed to the presence of defect band (D-band) because of the asymmetrical and symmetrical stretching of methylene and methyl groups [54]. Thus, the FT-IR result clearly indicated that the oxygen-containing functional groups were successfully created on the CB surface with 20% HNO_3 treatment.

Bulk structural information of the synthesized Ag/C catalyst was obtained using XRD as presented in Fig. 3. The broad peak at 2θ value of about 25° can be assigned to carbon (002) facet. The diffraction carbon peak at 25° was found to considerably decrease in Ag/C catalyst, indicating that there is a strong interaction between the CB support and deposited Ag nanoparticles resulting from good metal particle distribution on the carbon supporters. The peaks at 38.3, 44.2, 64.4, and 77.4° in the XRD pattern of Ag/C corresponding to the (111), (200), (220) and (311) planes, respectively, confirming the Ag nanoparticles' crystalline nature in the face-centered cubic (FCC) structure [56]. Moreover, the XRD pattern manifested that the Ag nanoparticles produced in the carbon-supported Ag catalyst are in metallic form since no characteristic oxide peak was found. The XRD analysis of the commercial nano-silver powder is also shown in this figure in which the peaks appeared at the same 2θ values as ones in the synthesized Ag/C. Hence, the XRD results confirmed the purity of the synthesized Ag particles supported onto carbon back surfaces.

The catalyst surface and elemental composition were further characterized using SEM, TEM, and Energy Dispersive X-Ray (EDX) analysis. The typical SEM micrographs and TEM images of synthesized Ag/C catalyst are presented in Figs. 4 and 5 Scanning electron micrographsand TEM images show that the Ag particles are heterogeneously dispersed on the CB of around 50 nm particle size with rare presence of aggregated silver nanoparticles, confirming the presence of Ag in the prepared catalysts with the nanoparticle size less than 20 nm. The corresponding EDX pattern (Fig. 6b) also indicates the presence of Ag nanoparticles in the synthesized Ag/C catalyst. In addition, the Ag content of the synthesized catalyst, determined from EDX analysis, is reported on the right side of the Fig. 6b. The result is close to the nominal one planed during the synthesis procedure.

To further determine the metal loading of Ag/C, TGA was carried out. Figure 7 shows the thermogravimetric graph of 40% Ag/C from room temperature (~ 27 °C) to 930 °C under N_2 and O_2 environments. The reasons for setting highest temperature (930 °C) in the TGA measurement are due to that carbon black particles will be completely burned at a temperature of around 920 °C [57] and that the melting point of pure silver is about 961 °C.The slight weight loss (~6.5%) from room temperature to 450 °C could be due to the loss of moisture and physical damages of the amorphous content in the catalyst [58]. The significant weight loss above 450 °C can be ascribed to the carbon black decomposition.

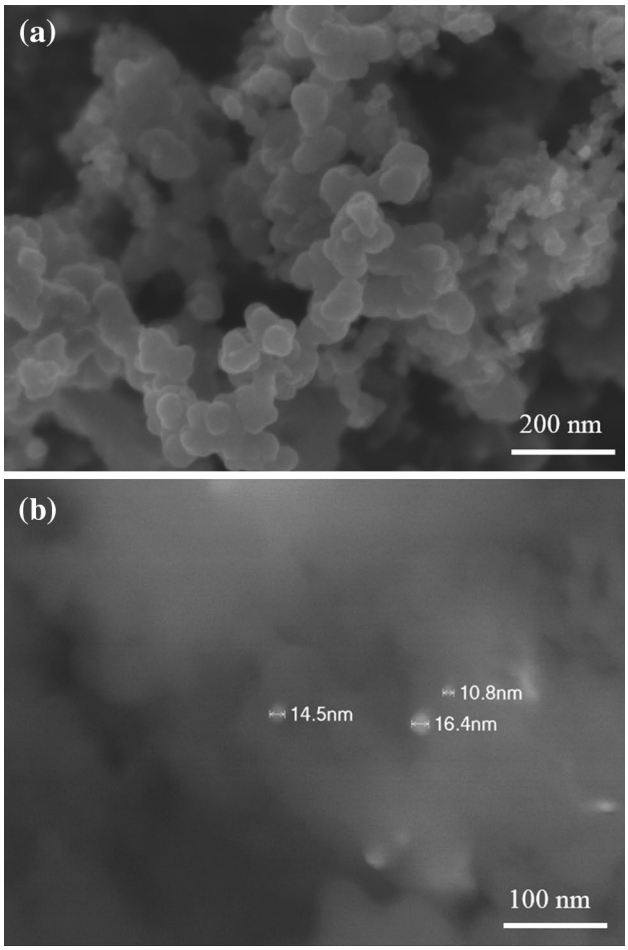

Fig. 4 Surface morphology SEM images of **a** Bare carbon black (SEI mode) and **b** Ag/C (COMPO mode)

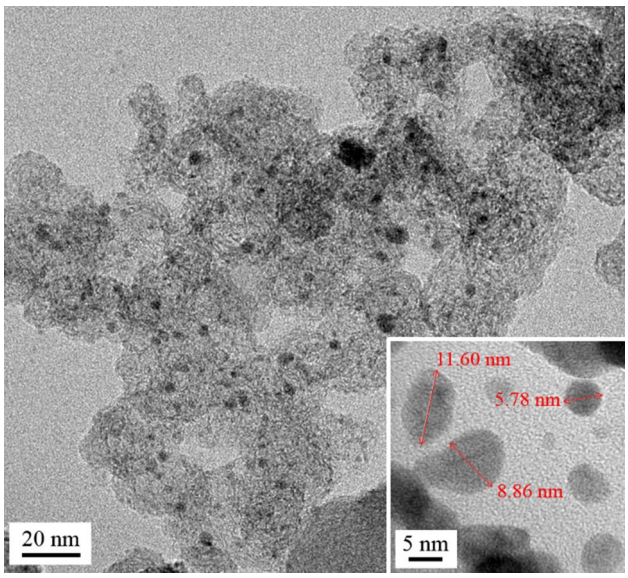

Fig. 5 TEM images of the Ag/C catalyst

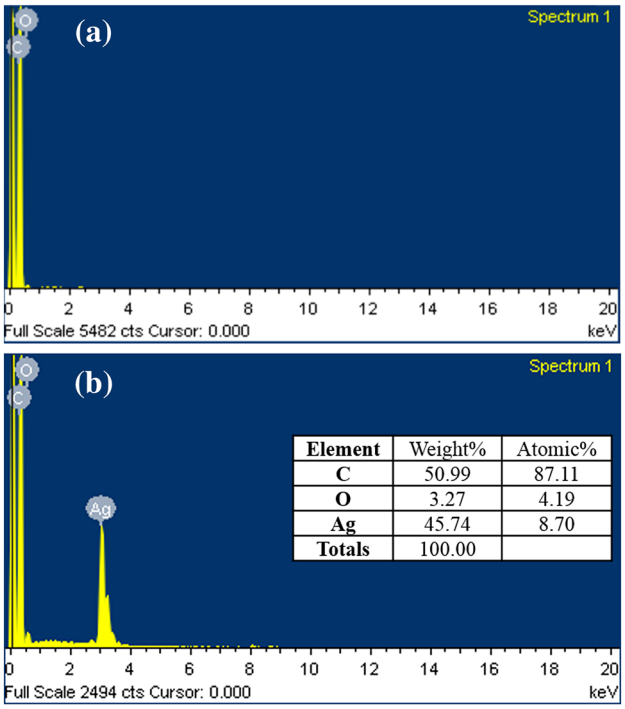

Element	Weight%	Atomic%
C	50.99	87.11
O	3.27	4.19
Ag	45.74	8.70
Totals	100.00	

Fig. 6 EDX pattern of **a** Bare CB, and **b** Ag/C

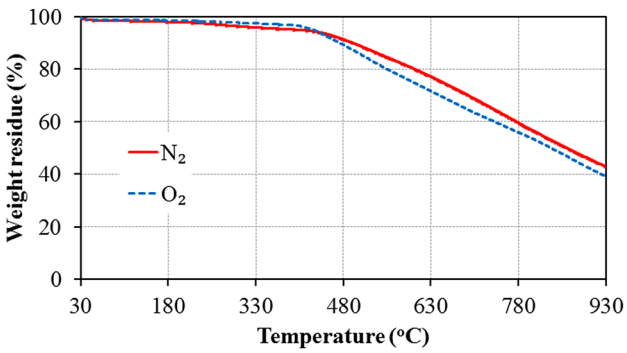

Fig. 7 Thermogravimetric analysis graph of prepared Ag/C catalyst

The results show that the retained weights of the analyzed samples were 42.9% and 39.2% at a temperature of 930 °C under N_2 and O_2 environments, respectively, which can be assigned to the Ag metal. This result is similar to the EDX data (45.7%). The slight difference between EDX and TGA analyses may be due to the heterogeneous distribution of Ag in the Ag/C catalyst among the analyzed samples.

Figure 8 shows the CVs of Pt/C, Ag/C, and commercial Ag catalysts in 1 M KOH solution. In the potential range between − 1.0 and 0.4 V vs. Ag/AgCl, three anodic peaks and one cathodic peak were observed at around 0.084, 0.124, 0.222, and − 0.015 vs. Ag/AgCl, respectively, which are in good agreement with those reported in the literature [59, 60]. Jovic et al. [61] have demonstrated that the two anodic

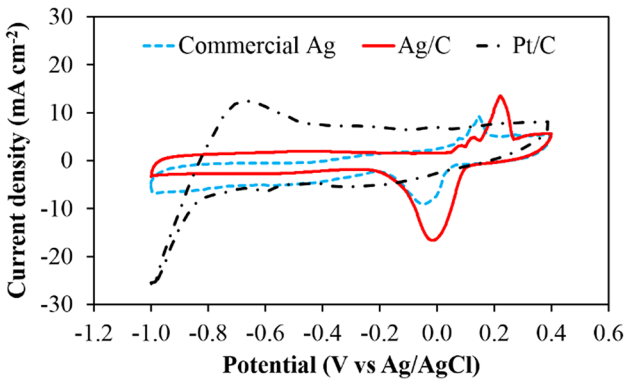

Fig. 8 Cyclic voltammograms of different catalysts for ORR in 1 M KOH at scan rate of 100 mVs^{-1}

peaks at around 0.124 and 0.222 V vs. Ag/AgCl could be ascribed to the formation of a compact and porous Ag_2O layer. The peak at 0.084 V vs. Ag/AgCl is due to the formation of a few monolayers of AgOH and Ag(I) species [31]. The electrochemical surface area (ESA) of these catalysts were calculated from CVs for comparison. The peak of hydrogen adsorption was used to estimate the ESA of Pt/C catalyst [62] while the ESAs of Ag/C and commercial Ag were determined from the oxide reduction peak of Ag(I) to Ag(0) due to lack of hydrogen adsorption peak [59]. The ESA of commercial Ag, Ag/C, and Pt/C were 51.9, 102.0, and 135.4 $m^2 g^{-1}$, respectively. Without carbon support and larger Ag nanoparticle size (around 20 nm), the commercial Ag catalyst showed the smallest ESA compared to the other two catalysts. In addition, a higher ESA of the Pt/C catalyst compared with the synthesized Ag/C catalyst can be attributed to the smaller size of Pt nanoparticles (< 5 nm from manufacturer).

To further assess the catalytic activity of the catalysts, the LSV using rotating disk electrode has been carried out in O_2-saturated 1 M KOH at a scan rate of 10 mV s^{-1} and the electrode's rotation rate of 2400 rpm, as shown in Fig. 9a. It can be seen that the onset potential and limiting diffusion current density of Ag/C are around 0.05 V and 3.1 mA.cm^{-2} which are slightly smaller than those of Pt/C (0.11 V and 3.3 mA cm^{-2}), respectively, indicating that the ORR activity of Ag/C is competitive to that of Pt/C. Figure 9b depicts the Tafel slopes of Pt/C, Ag/C, and commercial Ag catalysts. The Tafel slopes of Ag/C and Pt/C are − 121 and − 126 mV dec^{-1}, respectively, which are in agreement with data in the literature [20, 63, 64]. It is obvious that the Tafel slopes of Ag/C and Pt/C are very close, suggesting a similar mechanism for ORR in both catalysts. In addition, the Tafel slope values are ca. − 120 mV dec^{-1}, indicating that the first electron transfer step is the rate-determining step in ORR [20]. However, it was observed that commercial Ag has much lower onset potential and limiting diffusion current density

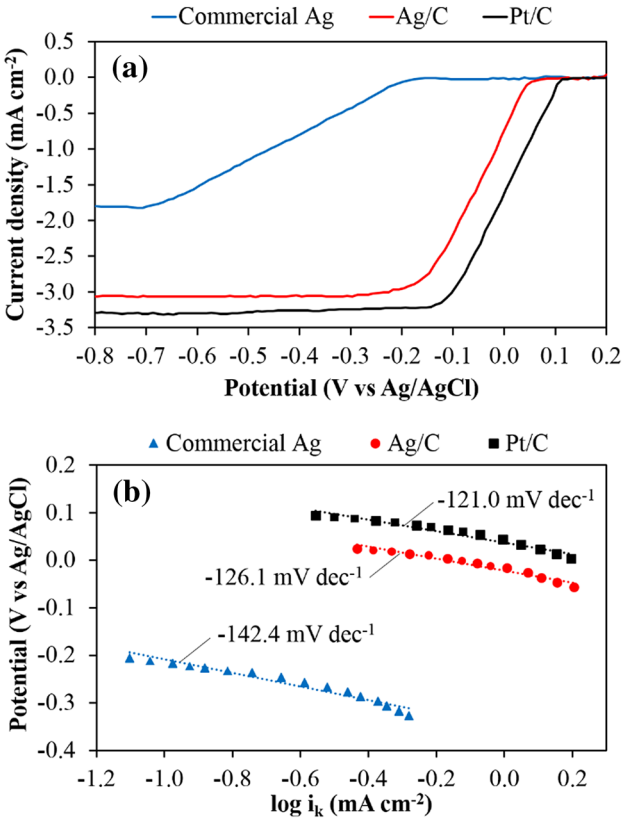

Fig. 9 Linear sweep voltammograms of different catalysts for ORR in O_2-saturated 1 M KOH. Scan rate: 10 mV s^{-1}. Rotation rate: 2400 rpm. **a** Steady state polarization curves; **b** Tafel plots

(− 0.2 V and 1.8 mA cm^{-2}, respectively) for ORR as well as larger Tafel slope (− 142.4 mV dec^{-1}), revealing that the commercial Ag has considerably lower activity compared to the two others. All the electrochemical parameters with error ranges derived from CV and LSV measurements are summarized in Table 1.

3.2 AEMFC Performance Results

Figure 10 shows the polarization and power density curves of the H_2/O_2 AEMFC single cell with commercial Ag nanoparticles, synthesized Ag/C or Pt/C used as the cathode

Table 1 Electrochemical parameters derived from CV and LSV measurements

Parameters	Commercial Ag	Ag/C	Pt/C
ESA ($m^2 g^{-1}$)	51.9 ± 3.6	102.0 ± 4.2	135.4 ± 5.1
Onset potential (V)	− 0.2 ± 0.018	0.05 ± 0.014	0.11 ± 0.011
Limiting diffusion current density (mA cm^{-2})	1.8 ± 0.05	3.1 ± 0.06	3.3 ± 0.04
Tafel slope (mV dec^{-1})	− 142.4 ± 2.1	− 121 ± 1.8	− 126 ± 1.9

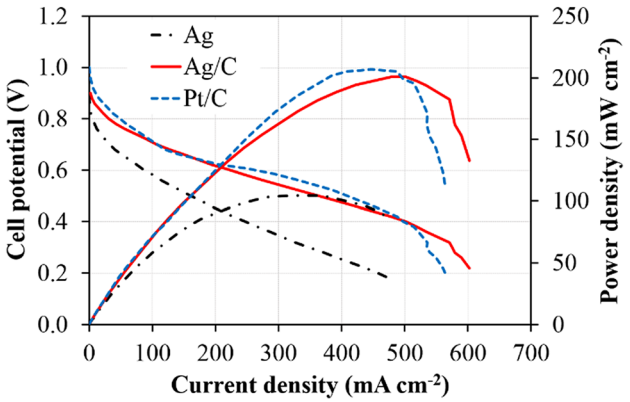

Fig. 10 AEMFC polarization and power density curves for different cathode catalysts

Table 2 The peak power density of AEMFC using different cathode catalysts

Catalyst	Commercial Ag	Ag/C	Pt/C
Peak power density ($mWcm^{-2}$)	105 ± 8	200 ± 6	207 ± 9

catalysts while anode catalyst was Pt/C in all tests. Such a single cell was operated at 50 °C under pure H_2 and O_2 gases of dew points of 50 and 55 °C, respectively. The peak power densities were 207 m Wcm^{-2}, 200 m Wcm^{-2} and 105 m Wcm^{-2} for Pt/C, Ag/C, and commercial nano-silver as summarized in Table 2, respectively. It can be seen that the synthesized 40 wt% Ag/C showed appreciated cell performance (only 3.5% lower) compared to commercial 40 wt% Pt/C. The slightly lower cell performance of using Ag/C as cathode catalyst can be attributed to the smaller ESA and ORR activity of Ag/C compared to Pt/C as discussed in CV and LSV results. This result suggested that Ag/C can be a competitive substitute to Pt/C as an AEMFC cathode catalyst. Besides, without a carbon supporter, the cell performance of nano-silver cathode electrode is about 2 times lower than that of synthesized Ag/C electrode, even though the nano-silver load (3.0 mg cm^{-2}) is much higher than the Ag/C (1.0 mg cm^{-2}) load in the cathode electrode, revealing the advantages of carbon support in synthesizing metal catalysts. This result is consistent with CV and LSV results.

Referring to material suppliers, the selling prices of the raw carbon black (Vulcan XC-72) is around 1 US$ per gram and the $AgNO_3$ material is around 2.7 US$ per gram as the purchasing amount is larger than 500 g. According to our catalyst synthesis procedure, the estimated cost will be approximately 3.6 US$ per gram for Ag/C industrial production. The price of the commercial Pt/C (40% wt% Pt/C, Tanaka) is about 80 US$ per gram. From the AEMFC performance results obtained in this work, the cost of using Ag/C as cathode catalyst is roughly 18 US$ per kW while it is almost 312 US$ per kW for using Pt/C. This indicates that an AEMFC with Ag/C cathode electrode will lead to an approximately 17-fold cost reduction to produce 1 kW compared with one with Pt/C cathode electrode.

4 Conclusions

Ag nanoparticles supported onto CB containing oxygen functional groups for the improvement of Ag dispersion were prepared using the impregnation method and studied. The XRD analysis revealed that the Ag catalyst which is in metallic form has been successfully deposited onto the carbon supporter. In addition, the EDX and TGA analyses indicated that the Ag content in the synthesized Ag/C is near the value designed in the synthesis procedure. The Ag nanoparticle size which is less than 20 nm was also observed from SEM and TEM images. The LSV measurements indicated that the ORR activities of Pt/C and as prepared Ag/C were comparable. The AEMFC performance using Ag/C or commercial Pt/C as the cathode catalyst in this study was very similar. The Pt/C power density of 207 m Wcm^{-2} is only about 3.5% higher than the Ag/C power density of 200 m Wcm^{-2}. Therefore, the catalyst on the cathode side can use the Ag/C catalyst to replace the Pt/C in strategic cost reduction, so that a commercialized alkaline anion exchange membrane fuel cell can be realized.

Acknowledgements This work is funded by the Ministry of Science and Technology of Taiwan under a Grant MOST-105-2923-E-005-001-MY3 and also supported in part by the Ministry of Education, Taiwan, R.O.C. under the Higher Education Sprout Project.

References

1. Steele, B. C. H., & Heinzel, A. (2001). Materials for fuel-cell technologies. *Nature, 414,* 345–352.
2. Hickner, M. A. (2010). Ion-containing polymers: New energy and clean water. *Materials Today, 13*(5), 34–41.
3. Cheema, T. A., Kim, G. M., Lee, C. Y., Kwak, M. K., Kim, H. B., & Park, C. W. (2014). Effects of composite porous gas-diffusion layers on performance of proton exchange membrane fuel cell. *International Journal of Precision Engineering and Manufacturing-Green Technology, 1*(4), 305–312.
4. Shin, D.-H., Yoo, S.-R. & Lee, Y.-H. (2019). Real time water contents measurement based on step response for PEM fuel cell. *International Journal of Precision Engineering and Manufacturing-Green Technology*.
5. Sik Kang, Y., Jo, S., Choi, D., Young Kim, J., Park, T. & Yoo, S. (2019). Pt-sputtered Ti mesh electrode for polymer electrolyte membrane fuel cells. *International Journal of Precision Engineering and Manufacturing-Green Technology*, *6*(2), 271–279.
6. Ho Seo, Y., Kim, J., Woong Ki, J., & Kim, B. (2014). Development of active breathing micro PEM fuel cell. *International Journal of Precision Engineering and Manufacturing-Green Technology, 1,* 101–106.

7. Lee, C.-W., Lee, M., Kang, M.-G., et al. (2018). Fabrication and operation characteristics of electrolyte impregnated matrix and cathode for molten carbonate fuel cells. *International Journal of Precision Engineering and Manufacturing-Green Technology, 5,* 279–286.
8. Hamad, T. A., Agll, A. A., Hamad, Y. M., et al. (2013). Study of a molten carbonate fuel cell combined heat, hydrogen and power system: end-use application. *Case Studies in Thermal Engineering, 1*(1), 45–50.
9. Son, J.-W., & Song, H.-S. (2014). Influence of current collector and cathode area discrepancy on performance evaluation of solid oxide fuel cell with thin-film-processed cathode. *International Journal of Precision Engineering and Manufacturing-Green Technology, 1*(4), 313–316.
10. Ji, S., Ha, J., Park, T., et al. (2016). Substrate-dependent growth of nanothin film solid oxide fuel cells toward cost-effective nanostructuring. *International Journal of Precision Engineering and Manufacturing-Green Technology, 3*(1), 35–39.
11. Choi, M., Lee, J. & Lee, W. (2019). Fluid mechanical approaches for rational design of infiltrated electrodes of solid oxide fuel cells. *International Journal of Precision Engineering and Manufacturing-Green Technology*, *6*(1), 53–61.
12. Neergat, M., & Shukla, A. K. (2001). A high-performance phosphoric acid fuel cell. *Journal of Power Sources, 102*(1), 317–321.
13. McLean, G. F., Niet, T., Prince-Richard, S., & Djilali, N. (2002). An assessment of alkaline fuel cell technology. *International Journal of Hydrogen Energy, 27*(5), 507–526.
14. Ge, X., Sumboja, A., Wuu, D., et al. (2015). Oxygen reduction in alkaline media: from mechanisms to recent advances of catalysts. *ACS Catal, 5*(8), 4643–4667.
15. Yang, W., Fellinger, T. P., & Antonietti, M. (2011). Efficient metal-free oxygen reduction in alkaline medium on high-surface-area mesoporous nitrogen-doped carbons made from ionic liquids and nucleobases. *Journal of the American Chemical Society, 133*(2), 206–209.
16. Hermann, A., Chaudhuri, T., & Spagnol, P. (2005). Bipolar plates for PEM fuel cells: a review. *International Journal of Hydrogen Energy, 30*(12), 1297–1302.
17. Sammes, N. (2006). *Fuel cell technology: reaching towards commercialization*. London: Springer.
18. Sljukic, P. B., Banks, C. G., & Compton, R. (2005). An overview of the electrochemical reduction of oxygen at carbon-based modified electrodes. *Journal of the Iranian Chemical Society, 2,* 1–25.
19. Xu, J., Gao, P., & Zhao, T. S. (2012). Non-precious Co3O4 nano-rod electrocatalyst for oxygen reduction reaction in anion-exchange membrane fuel cells. *Energy & Environmental Science, 5*(1), 5333–5339.
20. Qaseem, A., Chen, F., Wu, X., & Johnston, R. L. (2016). Pt-free silver nanoalloy electrocatalysts for oxygen reduction reaction in alkaline media. *Catalysis Science & Technology, 6*(10), 3317–3340.
21. Coutanceau, C., Demarconnay, L., Lamy, C., & Léger, J. M. (2006). Development of electrocatalysts for solid alkaline fuel cell (SAFC). *Journal of Power Sources, 156*(1), 14–19.
22. Spendelow, J. S., & Wieckowski, A. (2007). Electrocatalysis of oxygen reduction and small alcohol oxidation in alkaline media. *Physical Chemistry Chemical Physics: PCCP, 9*(21), 2654–2675.
23. Barsuk, D., Zadick, A., Chatenet, M., et al. (2016). Nanoporous silver for electrocatalysis application in alkaline fuel cells. *Materials and Design, 111,* 528–536.
24. Bidault, F., & Kucernak, A. (2010). A novel cathode for alkaline fuel cells based on a porous silver membrane. *Journal of Power Sources, 195*(9), 2549–2556.
25. Chatenet, M., Genies-Bultel, L., Aurousseau, M., Durand, R., & Andolfatto, F. (2002). Oxygen reduction on silver catalysts in solutions containing various concentrations of sodium hydroxide—comparison with platinum. *Journal of Applied Electrochemistry, 32,* 1131–1140.
26. Wang, Y., Liu, Y., Lu, X., et al. (2012). Silver-molybdate electrocatalysts for oxygen reduction reaction in alkaline media. *Electrochemistry Communications, 20,* 171–174.
27. Meng, H., & Shen, P. K. (2006). Novel Pt-free catalyst for oxygen electroreduction. *Electrochemistry Communications, 8*(4), 588–594.
28. Blizanac, B. B., Ross, P. N., & Marković, N. M. (2006). Oxygen reduction on silver low-index single-crystal surfaces in alkaline solution: rotating ring DiskAg(hkl) studies. *The Journal of Physical Chemistry B, 110*(10), 4735–4741.
29. Han, J.-J., Li, N., & Zhang, T.-Y. (2009). Ag/C nanoparticles as an cathode catalyst for a zinc-air battery with a flowing alkaline electrolyte. *Journal of Power Sources, 193*(2), 885–889.
30. Xin, L., Zhang, Z., Wang, Z., Qi, J. and Li, W. (2013). Carbon supported Ag nanoparticles as high performance cathode catalyst for H_2/O_2 anion exchange membrane fuel cell. *Frontiers in Chemistry*, *1*(16), 1–5.
31. Garcia, A. H. S., Gasparotto, L. F., Gomes, J., & Tremiliosi-Filho, G. (2012). Straightforward synthesis of carbon-supported Ag nanoparticles and their application for the oxygen reduction reaction. *Electrocatalysis, 3,* 147–152.
32. Vinodh, R., & Sangeetha, D. (2012). Carbon supported silver (Ag/C) electrocatalysts for alkaline membrane fuel cells. *Journal of Materials Science, 47,* 852–859.
33. Maheswari, S., Sridhar, P., & Pitchumani, S. (2012). Carbon-supported silver as cathode electrocatalyst for alkaline polymer electrolyte membrane fuel cells. *Electrocatal, 3,* 13–21.
34. Wang, Z., Xin, L., Zhao, X., et al. (2014). Carbon supported Ag nanoparticles with different particle size as cathode catalysts for anion exchange membrane direct glycerol fuel cells. *Renewable Energy, 62,* 556–562.
35. Arukula, R., Vinothkannan, M., Kim, A. R., & Yoo, D. J. (2019). Cumulative effect of bimetallic alloy, conductive polymer and graphene toward electrooxidation of methanol: An efficient anode catalyst for direct methanol fuel cells. *Journal of Alloys and Compounds, 771,* 477–488.
36. Ramakrishnan, S., Karuppannan, M., Mohanraj, V., Ramachandran, K., Kwon, O. J., & Yoo, D. J. (2019). Ultrafine Pt nanoparticles stabilized by MoS2/N-doped reduced graphene oxide as a durable electrocatalyst for alcohol oxidation and oxygen reduction reactions. *ACS Applied Materials & Interfaces, 11,* 12504–12515.
37. Bala, T., Prasad, B. L. V., Sastry, M., Kahaly, M. U., & Waghmare, U. V. (2007). Interaction of different metal ions with carboxylic acid group: A quantitative study. *The Journal of Physical Chemistry A, 111*(28), 6183–6190.
38. Rivas, B. L., Pereira, E. D., & Moreno-Villoslada, I. (2003). Water-soluble polymer–metal ion interactions. *Progress in Polymer Science, 28*(2), 173–208.
39. Yang, Y., Chiang, K., & Burke, N. (2011). Porous carbon-supported catalysts for energy and environmental applications: A short review. *Catalysis Today, 178*(1), 197–205.
40. Chen, J. P., & Wu, S. (2004). Acid/base-treated activated carbons: Characterization of functional groups and metal adsorptive properties. *Langmuir, 20*(6), 2233–2242.
41. Bhatnagar, A., Hogland, W., Marques, M., & Sillanpää, M. (2013). An overview of the modification methods of activated carbon for its water treatment applications. *Chemical Engineering Journal, 219,* 499–511.
42. Boudou, J. P., Paredes, J. I., Cuesta, A., Martínez-Alonso, A., & Tascón, J. M. D. (2003). Oxygen plasma modification of pitch-based isotropic carbon fibres. *Carbon, 41*(1), 41–56.
43. Xie, F., Phillips, J., Silva, I. F., Palma, M. C., & Menéndez, J. A. (2000). Microcalorimetric study of acid sites on ammonia- and acid-pretreated activated carbon. *Carbon, 38*(5), 691–700.

44. Hu, C.-C., & Wang, C.-C. (2004). Effects of electrolytes and electrochemical pretreatments on the capacitive characteristics of activated carbon fabrics for supercapacitors. *Journal of Power Sources, 125*(2), 299–308.
45. Sosa, R. C., Parton, R. F., Neys, P. E., Lardinois, O., Jacobs, P. A., & Rouxhet, P. G. (1996). Surface modification of carbon black by oxidation and its influence on the activity of immobilized catalase and iron-phthalocyanines. *Journal of Molecular Catalysis A: Chemical, 110*(2), 141–151.
46. Zhou, D.-M., Wang, Y.-J., Wang, H.-W., Wang, S.-Q., & Cheng, J.-M. (2010). Surface-modified nanoscale carbon black used as sorbents for Cu(II) and Cd(II). *Journal of Hazardous Materials, 174*(1), 34–39.
47. Carmo, M., Linardi, M., & Poco, J. G. R. (2009). Characterization of nitric acid functionalized carbon black and its evaluation as electrocatalyst support for direct methanol fuel cell applications. *Applied Catalysis, A: General, 355*(1), 132–138.
48. Aksoylu, A. E., Madalena, M., Freitas, A., Pereira, M. F. R., & Figueiredo, J. L. (2001). The effects of different activated carbon supports and support modifications on the properties of Pt/AC catalysts. *Carbon, 39*(2), 175–185.
49. Xiong, H., Nolan, M., Shanks, B. H., & Datye, A. K. (2014). Comparison of impregnation and deposition precipitation for the synthesis of hydrothermally stable niobia/carbon. *Applied Catalysis, A: General, 471,* 165–174.
50. Quintanilla, A., Casas, J. A., & Rodríguez, J. J. (2007). Catalytic wet air oxidation of phenol with modified activated carbons and Fe/activated carbon catalysts. *Applied Catalysis, B: Environmental, 76*(1), 135–145.
51. Prado-Burguete, C., Linares-Solano, A., Rodríguez-Reinoso, F., & de Lecea, C. S.-M. (1989). The effect of oxygen surface groups of the support on platinum dispersion in Pt/carbon catalysts. *Journal of Catalysis, 115*(1), 98–106.
52. Ahmed, D. S., Haider, A. J., & Mohammad, M. R. (2013). Comparesion of functionalization of multi-walled carbon nanotubes treated by oil olive and nitric acid and their characterization. *Energy Procedia, 36,* 1111–1118.
53. Le, V. T., Ngo, C. L., Le, Q. T., Ngo, T. T., Nguyen, D. N., & Vu, M. T. (2013). Surface modification and functionalization of carbon nanotube with some organic compounds. *Advances in Natural Sciences: Nanoscience and Nanotechnology, 4*(3), 035017.
54. Mohan, A. N. (2012). Synthesis and characterization of carbon nanospheres from hydrocarbon soot. *International Journal of Electrochemical Science, 7,* 9537–9549.
55. Rios, R. R. A., Alves, D. E., Dalmázio, I., Bento, S. F. V., Donnici, C. L., & Lago, R. M. (2003). Tailoring activated carbon by surface chemical modification with O, S, and N containing molecules. *Materials Research, 6,* 129–135.
56. Singh, P., Kim, Y. J., Singh, H., et al. (2015). Biosynthesis, characterization, and antimicrobial applications of silver nanoparticles. *International Journal of Nanomedicine, 10,* 2567–2577.
57. Wang, W., Wang, Z., Wang, J., Zhong, C.-J., & Liu, C.-J. (2017). Highly active and stable Pt-Pd alloy catalysts synthesized by room-temperature electron reduction for oxygen reduction reaction. *Advanced Science, 4*(4), 1600486.
58. Alimohammadi, F., Gashti, M. P., Shamei, A., & Kiumarsi, A. (2012). Deposition of silver nanoparticles on carbon nanotube by chemical reduction method: Evaluation of surface, thermal and optical properties. *Superlattices and Microstructures, 52*(1), 50–62.
59. Maheswari, S., Parthasarathi, S., & Pitchumani, S. (2012). Carbon-supported silver as cathode electrocatalyst for alkaline polymer electrolyte membrane fuel cells. *Electrocatalysis, 3,* 13–21.
60. Guo, J., Hsu, A., Chu, D., & Chen, R. (2010). Improving oxygen reduction reaction activities on carbon-supported Ag nanoparticles in alkaline solutions. *Journal of Physical Chemistry C, 114*(10), 4324–4330.
61. Jović, B., & Jovic, V. (2004). Electrochemical formation and characterization of Ag2O. *Journal of the Serbian Chemical Society, 69*(2), 153–166.
62. Mahapatra, S. S., & Datta, J. (2011). Characterization of Pt-Pd/C electrocatalyst for methanol oxidation in alkaline medium. *International Journal of Electrochemistry, 1–16,* 2011.
63. Wiberg, G. K. H., Mayrhofer, K. J. J., & Arenz, M. (2010). Investigation of the oxygen reduction activity on silver—a rotating disc electrode study. *Fuel Cells, 10*(4), 575–581.
64. Genies, L., Bultel, Y., Faure, R., & Durand, R. (2003). Impedance study of the oxygen reduction reaction on platinum nanoparticles in alkaline media. *Electrochimica Acta, 48*(25), 3879–3890.

Van Men Truong is currently PhD candidate under the supervision of Professor Hsiharng Yang in the Graduate Institute of Precision Engineering at National Chung Hsing University in Taiwan. He received his bachelor degree in mechanical engineering from Nong Lam University-Ho Chi Minh City, Vietnam in 2005. After graduation, he worked for TraVinh University, Vietnam as a lecturer and research assistant. He completed his Master of Science degree in mechanical engineering at National Chung Hsing University, Taiwan in 2015. His current research focuses on the development of non-PGM electrodes for anion exchange membrane fuel cells.

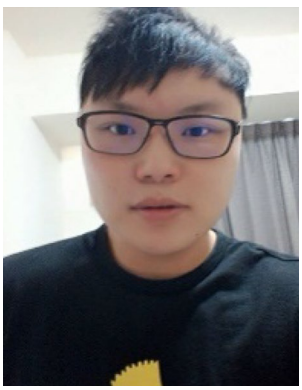

Ming-Kun Yang graduated from the Graduate Institute of Precision Engineering at National Chung Hsing University in Taiwan (2018). His research focuses on the development of non-PGM electrodes for anion exchange membrane fuel cells.

Hsiharng Yang is a Tenured Distinguished Professor in the Graduate Institute of Precision Engineering at National Chung Hsing University (NCHU) in Taiwan. He studied in the Institute for Micromanufacturing at Louisiana Tech University and graduated in 1998. He was a researcher in the Industrial Technology Research Institute working on MEMS related products. In 2000, he joined the Graduate Institute of Precision Engineering at NCHU as an Assistant Professor. He has been an Associate Professor and full Professor in 2006. His current research interests include anion exchange membrane fuel cells, enzymatic biofuel cells, carbon fiber related electrodes, gas diffusion electrodes.